Cartesion Prime PET/CT: Time-of-Flight Technology

Yibao Wu, PhD, Medical Affairs Manager
Maria Iatrou, PhD, MBA, Medical Affairs Leader
Canon Medical Systems USA

Introduction

Over the last two decades, tremendous advancements in new instrumentation, data processing technologies, new imaging tracers and radiolabeled therapeutic molecules have accommodated the rapidly growing role of PET in patient care and the evolution of precision medicine. One of these technical developments, time-of-flight (TOF) PET, enables the measurement of the difference between the arrival times of two 511 keV photons at paired detectors. In non-TOF PET, emitted activity is assumed to be uniformly distributed along the line of response (LOR) between a detector pair due to lack of TOF information (Figure 1A). With TOF, the difference between the arrival times of two photons at paired detectors is used to pinpoint the location of the annihilation of the radioactivity (Figure 1B).

The position uncertainty of the annihilation event is given by the following equation:

$$x = \frac{c\Delta t}{2} \quad (1),$$

where c is the speed of light and Δt the TOF resolution.

Incorporation of TOF information in image reconstruction improves count localization, noise correlation, signal-to-noise ratio (SNR), contrast recovery and effective sensitivity, especially for larger patients.[1-4] Under clinical protocols, TOF PET also results in improved accuracy and precision of the measured activity in small lesions across subjects and within a subject.[4] In addition, TOF PET imaging is less sensitive to errors in data corrections and mismatch between the CT attenuation map and PET image.[5]

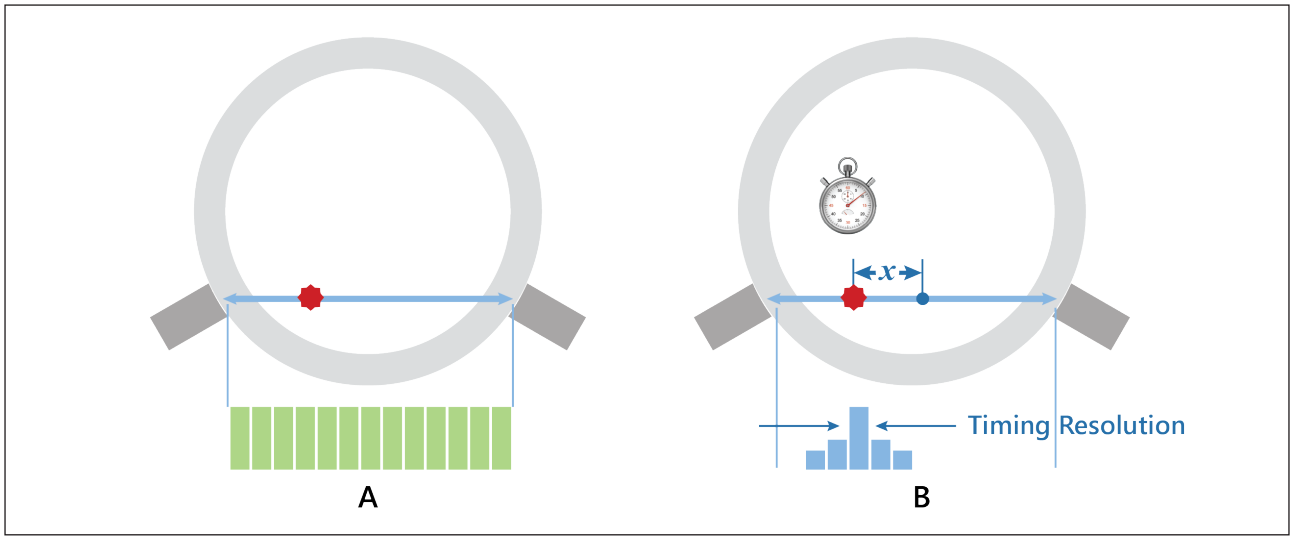

Figure 1 Illustration of PET without (A) and with (B) TOF capabilities.

Cartesion Digital PET/CT

- Digital PET detector
- 263 ps Time-of-Flight resolution (typical)
- Air-cooled detector
- 1:1 coupling of crystal to SiPM
- 100% SiPM coverage
- 27 cm axial FOV

- Aquilion Prime SP CT
- Standard Technologies:
  - AIDR 3D dose reduction
  - SEMAR, metal artifact reduction
  - Time-of-Flight
  - Point Spread Function (PSF) reconstruction

Figure 2 Cartesion Prime Digital PET/CT

TOF technology, commercially available with LSO crystals since the mid-2000s, has been combined more recently with digital PET SiPM technology. Canon Medical's Cartesion Prime PET/CT is a digital PET/ CT system with excellent TOF resolution. Figure 2 summarizes Cartesion's major performance specs and features.[6-7]

Cartesion Prime PET/CT TOF Detector

PET detector design impacts the performance of PET systems. PET detectors use scintillators to convert gamma ray photons to light output. Table 1 lists the key properties of some PET scintillators.[8] The first generation of TOF PET scanners was built in the 1980s using fast scintillators such as CsF and BaF_2.[9] Although timing resolution was sufficient, the low stopping power and weak light output made these scintillators less efficient. BGO detectors, which were developed shortly after, have much higher stopping power and acceptable light output. BGO crystals became the standard material for PET detectors for many years. However, due to the long decay time and low light output, BGO was not used for TOF PET. The discovery of Lutetium-based scintillators, such as LSO and LYSO, prompted the development of a new generation of PET scanners. These scintillators have short decay time and can be used for TOF PET. And unlike TOF scintillators used in the 1980s, they have high stopping power and very good light output. As a result, the efficiency of the detector is not compromised.

	NaI (Tl)	BaF_2	BGO	LSO	LYSO
Effective Z	51	54	74	66	60
Linear attenuation coefficient (cm^{-1})	0.34	0.44	0.92	0.87	0.86
Density (g/cm^3)	3.67	4.89	7.13	7.4	7.1
Light yield (% NaI(Tl))	100	5	15	75	80
Decay constant (ns)	230	0.8	300	40	41

Table 1 Properties of some PET scintillators.

Canon Medical Systems' Cartesion PET/CT detector uses Lutetium-based scintillator combined with SiPM technology and offers a 27-cm axial field of view (FOV) with 263 ps (typical) TOF resolution. It was designed to achieve better image quality, improve throughput, optimize dose, and reduce total cost of ownership. Figure 3 shows the detector design. Each SiPM is coupled to a Lutetium-based scintillator. The size of the scintillator crystal is an important parameter of the system design. Smaller pixels improve spatial resolution, at the expense of reduced sensitivity. The thickness of the crystals also affects scanner performance. Thicker crystals have higher sensitivity, but spatial resolution and timing resolution deteriorate. Cartesion Prime incorporates a 4.1 x 4.1 x 20 mm^3 Lutetium-based scintillator crystal design that balances the various requirements and optimizes the performance of the detector. A 3 x 6 crystal-SiPM array is attached to a readout ASIC. A detector module contains eight such arrays placed in a 4 x 2 configuration totaling 12 x 12 channels. Finally, five modules are assembled in the axial direction forming a detector unit. This detector design has the following features: 27 cm long axial FOV, one-to-one crystal-SiPM coupling, 100% coverage of scintillator area, 263 ps TOF (typical), and air-cooling.

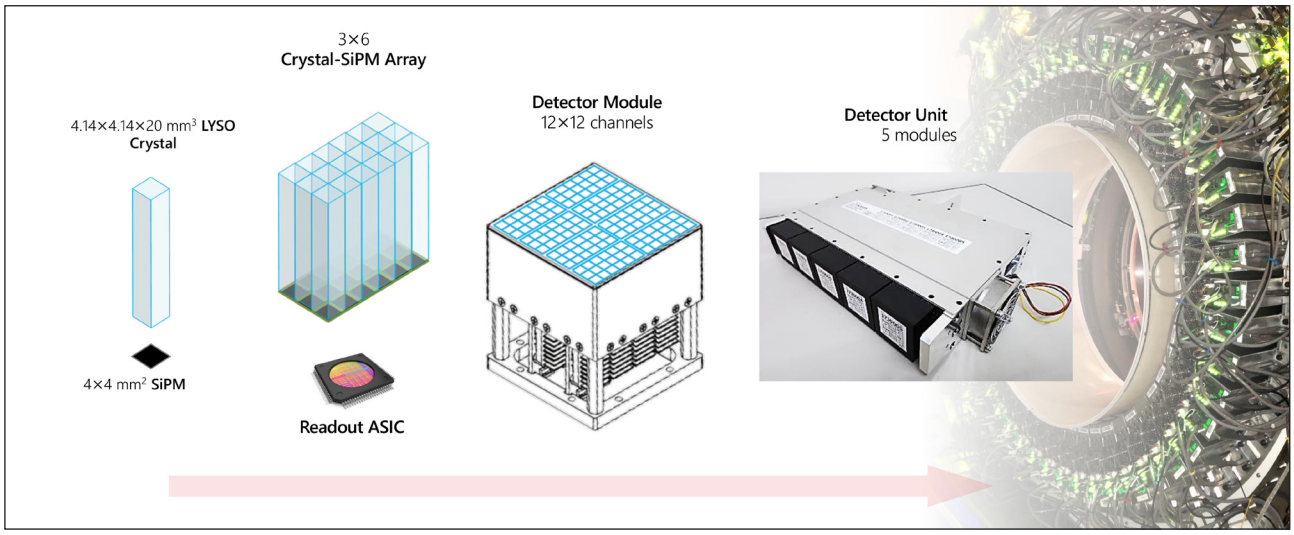

Figure 3 Cartesion Prime detector design.

TOF Gain and Effective Sensitivity

Theoretically, if the arrival time difference Δt could be measured perfectly, each coincidence event could be placed back to the source location and no tomographic reconstruction algorithm would be needed. To understand the SNR benefit of TOF, let's assume that an analytic reconstruction algorithm, such as filtered backprojection (FBP), is applied to the data. In FBP the projection data is filtered, then backprojected to image space. The value of each image pixel along the LOR (Figure 1A) is increased by an amount proportional to the number of events measured between the two detectors at the ends of the LOR. All the events recorded in the LOR contribute equally to all the pixels along the LOR and add noise to the pixels. Whereas in TOF PET, the contribution of each emission event to each pixel is weighted by the probability of a Gaussian distribution with FWHM of x (Figure 1B), where x is the position uncertainty. The better the TOF resolution, the smaller the spatial uncertainty and the smaller the FWHM of the Gaussian weighting probability. As a result, events only contribute to pixels near the pixel of their origin and add noise only to them. Consequently, TOF signal-to-noise ratio (SNR_{TOF}) is improved compared to non-TOF signal-to-noise ratio ($SNR_{non\text{-}TOF}$). The ratio of the TOF to the non-TOF variance is referred to as TOF gain and can be expressed as[10]:

$$\frac{SNR^2_{TOF}}{SNR^2_{non-TOF}} = \frac{2D}{c\Delta t} = \frac{D}{x} \quad (2)$$

The above TOF gain was originally derived for the central pixel in a uniform disk source scanned using 2D PET and reconstructed using FBP. Later experiments on modern 3D PET scanners using iterative reconstruction algorithms show similar results for both phantom and clinical patient studies.[5,11-13] TOF gain also increases as randoms ratio increases.[14] An updated estimate of TOF gain is given by equation[13] (3):

$$\frac{SNR^2_{TOF}}{SNR^2_{non-TOF}} = \frac{D}{1.6x} \quad (3)$$

Figure 4 shows the TOF gain for different combinations of object size and timing resolution estimated by equation (3). Cartesion Prime, Cannon's digital PET/CT scanner, has a typical timing resolution of 263 ps[6] resulting in a spatial uncertainty of less than 4 cm and typical TOF gain of 7.9 for a 50 cm diameter object. In comparison, the spatial uncertainty at a timing resolution of 500 ps is approximately 7.5 cm. The TOF gain achieved at a resolution of 500 ps is approximately 53% of the TOF gain achieved at 263 ps. TOF gains at 400 ps and 350 ps are 66% and 75% of that at 263 ps, respectively. Non-TOF detectors don't benefit from TOF gain.

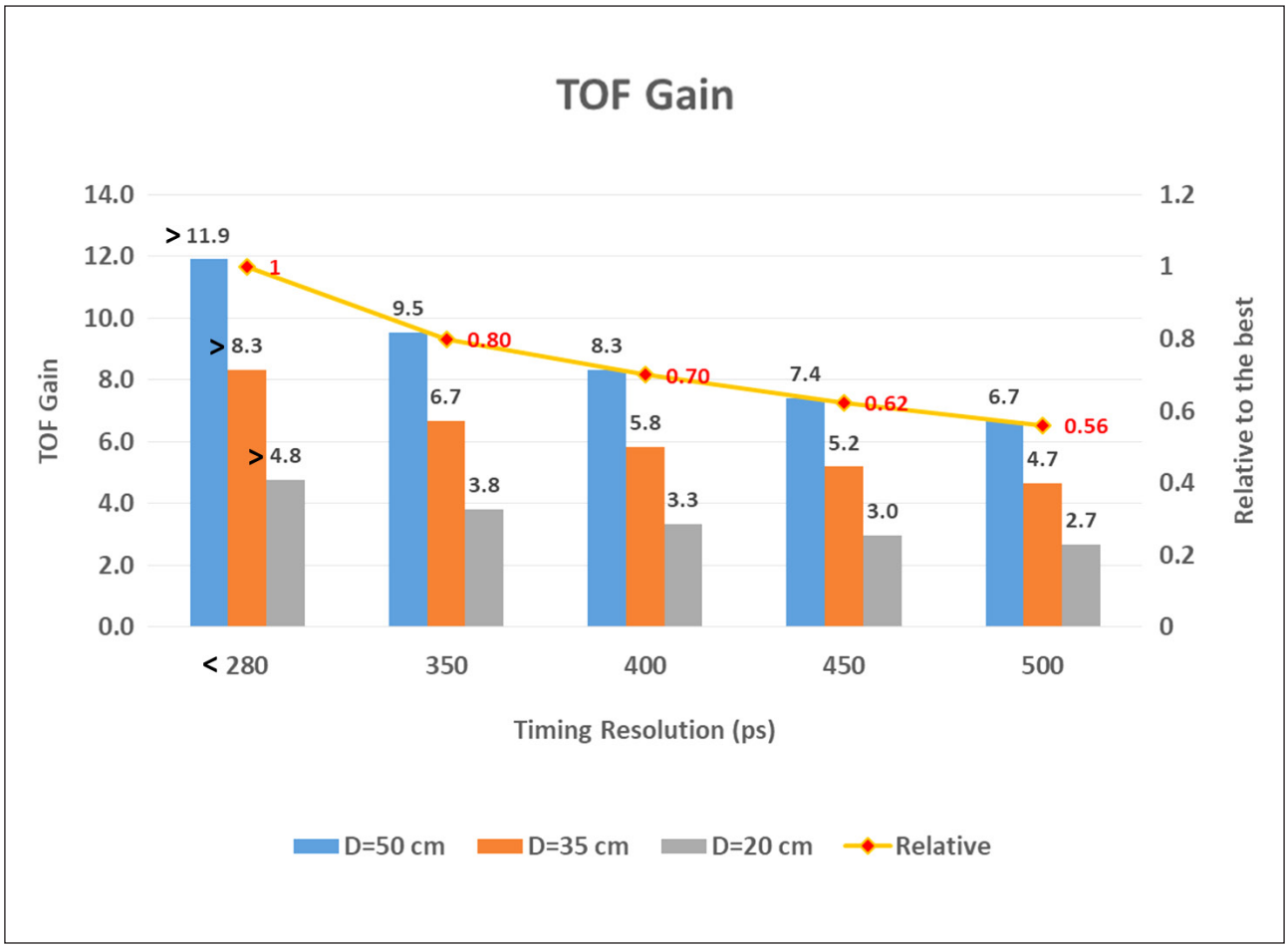

Figure 4 TOF gain for different object sizes and timing resolutions.

The product of NEMA sensitivity and TOF gain is called TOF effective sensitivity. Improved TOF gain results in improved effective sensitivity with a larger benefit demonstrated in imaging of larger patients. In non-TOF the effective sensitivity of a detector is equal to the sensitivity of the detector.

Evaluation of TOF Benefits

To demonstrate the improvement to image quality using TOF, a 35cm diameter cylindrical phantom was scanned on Cartesion Prime. Twelve spherical inserts with extension rods were attached to the removable cap of the phantom in two radii. Six spheres with inner diameters between 10 mm and 37 mm were inserted in the inner radius (about 6 cm from the sphere centers to the center of the phantom). Another six spheres with inner diameters of between 3.95 mm and 13 mm were inserted in the outer radius (about 10 cm from the sphere center to the center of the phantom).

18F-FDG solution was injected into the background and spheres. The phantom was positioned such that the centers of the spheres were located in the axial center of the scanner FOV. The phantom was scanned for 2 minutes and 11 minutes respectively. The background activity concentration was 5.2 kBq/cc at the beginning of the scan and the sphere-to- background concentration ratio was 7.6.

The data was reconstructed using a 3D listmode OSEM algorithm with and without TOF, two to sixteen iterations, twelve subsets, and Gaussian postfiltering with 4 mm FWHM. A 13 mm diameter spherical region of interest (ROI)

was drawn on the 13 mm hot sphere in the inner circle (Figure 6) and the mean activity concentration μH was measured. A 30 mm diameter spherical ROI was drawn in the central background area of the phantom, at least 25 mm away from all the spheres. The mean activity concentration μB and standard deviation σB of the background ROI were measured. The contrast recovery coefficient (CRC) and noise were given by:

$$CRC = \frac{(\mu H - \mu B)/\mu B}{C} \quad (4)$$

where

$$C = (aH - aB)/aB \quad (5)$$

$$Noise = \sigma_B/\mu_B \quad (6)$$

In eq. (5) aH and aB denotes the ground-truth activity concentration in hot spheres and background, respectively. Figure 5 shows the CRC vs. noise measurements. First, it is observed that the TOF reconstruction converges faster. After three iterations, the TOF image is very close to the peak CRC value. With non-TOF, at least eleven iterations are necessary to achieve near peak CRC. Second, it is noted that at two minutes of acquisition and the noise level reached at three iterations for TOF, the CRC for TOF is almost 70% higher than the CRC for non-TOF at the same noise level. Higher CRC at the same noise level results in better image quality. The 11-minute non-TOF curve shows that non-TOF CRC after twelve iterations is lower than the 2-minute TOF CRC after three iterations. Using the TOF gain equation (3) and the measured TOF resolution of 263 ps, the time reduction factor using TOF (TOF gain) is calculated as:

$$TOF\ gain = 2 \times 35(cm)/[1.6 \times 0.03(cm/ps) \times 263(ps)] = 5.5$$

The CRC vs. noise curves in Figure 5 show that the TOF gain is slightly better than 5.5, which is consistent with the estimation provided by equation (3). Figure 6 shows on the left the TOF image of a 2-minute scan reconstructed with 3 iterations and on the right the non-TOF of an 11-minute scan and reconstructed with 12 iterations. Both were reconstructed with 12 subsets and 4mm Gaussian post filter. Similar image quality is seen in both images, while the TOF acquisition time is 5.5 times shorter than the respective non-TOF acquisition time.

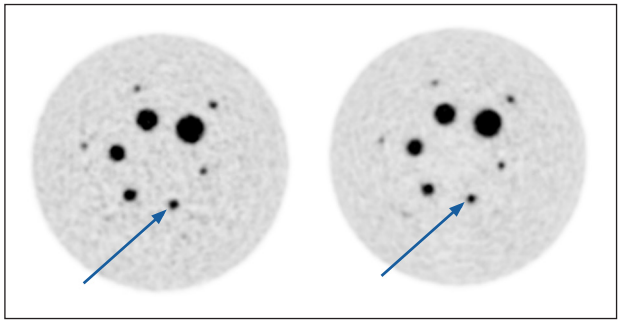

Figure 6 TOF image from a 2-minute scan (left) and non-TOF image from an 11-minute scan (right).

Further improvement in CRC at the same noise levels can be achieved with point spreading function (PSF) modeling in the reconstruction, as shown in Figure 7.

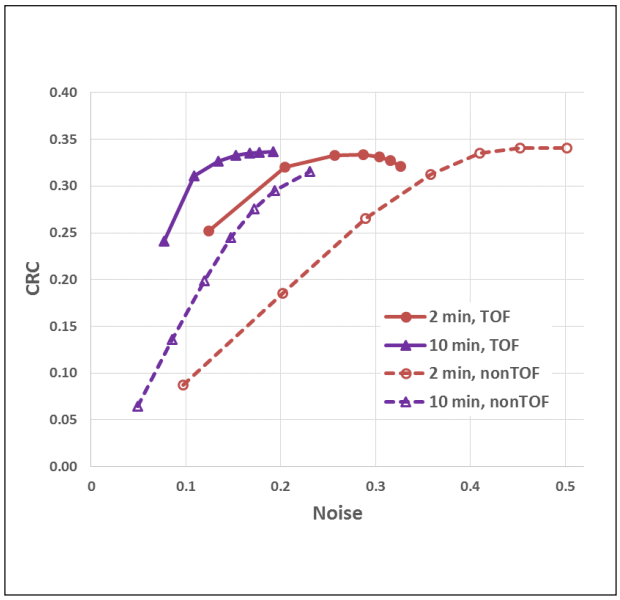

Figure 5 Contrast vs. noise plot for the 13 mm diameter sphere in the 35 cm diameter cylindrical phantom scanned on Cartesion and reconstructed without PSF.

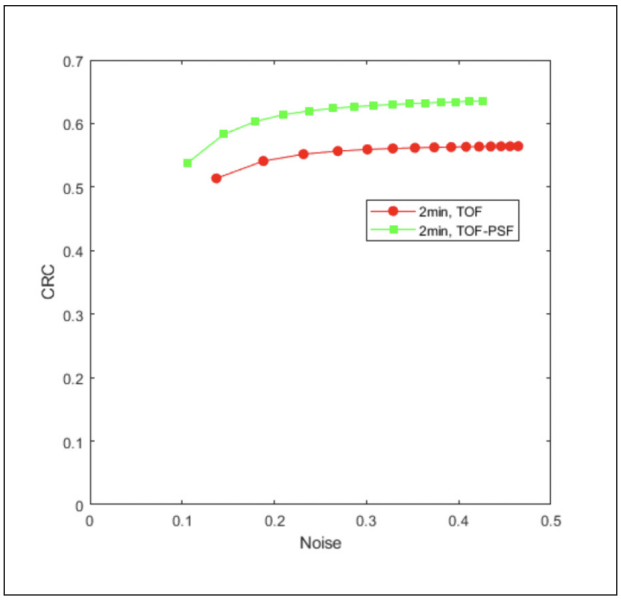

Figure 7 Contrast vs. noise plot for the 13 mm diameter sphere in the 35 cm diameter cylindrical phantom scanned on Cartesion and reconstructed with TOF and with (green) and without PSF (red).

A patient (BMI 45.1) was injected with 7.3 mCi and scanned with Cartesion PET/CT after 62 minutes of uptake. The images reconstructed with TOF and nonTOF are shown in Figure 8. Better contrast and higher SUVmax value were observed with TOF reconstruction.

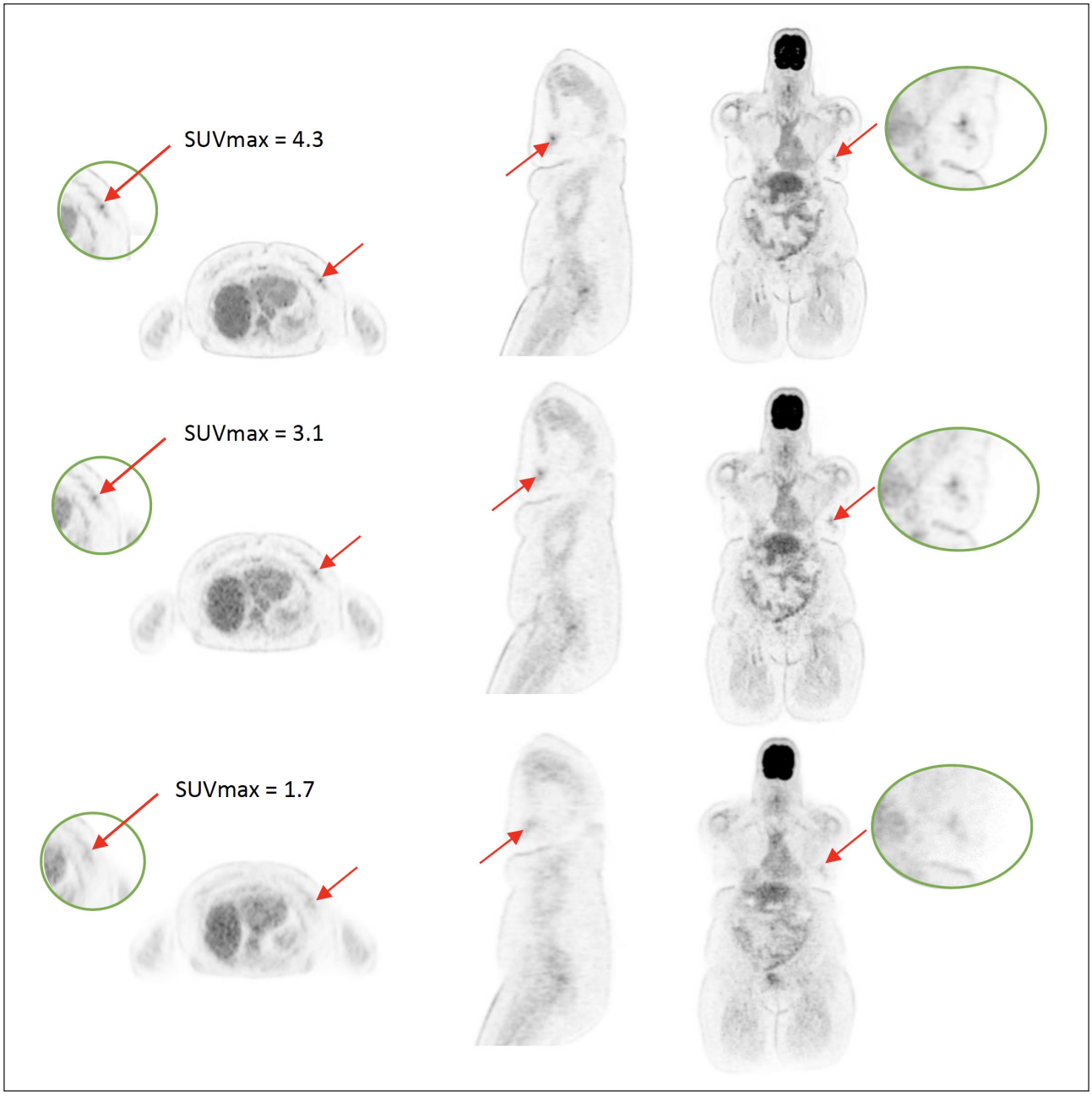

Figure 8 Patient images reconstructed with TOF AiCE (top), PSF TOF OSEM (middle) and OSEM without TOF (bottom).

Advanced intelligent Clear-IQ Engine (AiCE) for PET

In addition to TOF iterative reconstruction (OSEM) with point spread function modeling, Cartesion Prime also offers Deep Learning Reconstruction (DLR) technology, called Advanced intelligent Clear-IQ Engine (AiCE), for CT[14] and PET.[15,16] AiCE for PET yields superior performance compared to Gaussian post-filtered OSEM with point-spread-function by better differentiating signal from noise and generating high-quality images. Phantom studies with the NEMA image quality phantom have demonstrated improvements in image quality, quantification accuracy and preservation of SNR at reduced counts, or equivalently scan duration.[16]

Similar improvements in image quality are observed in clinical studies. Figure 9 shows the whole body ^{18}F-FDG images of a large patient (BMI 39.2) with primary lung

adenocarcinoma and DCIS of right breast. Patient was injected with 266 MBq (7.2 mCi) of ^{18}F-FDG and was scanned on a Cartesion Prime PET/CT after 53 minutes. The scan protocol comprised 5 beds with a 2-minute acquisition per bed and 50% bed overlap. Images were reconstructed using AiCE and OSEM with PSF, 4 iterations and 12 subsets, followed by a Gaussian filter with 6 mm FWHM. AiCE images show improved sharpness of the low contrast lesion in the outer right breast and multiple clusters of mediastinal lymph nodes. SUVmax of the low contrast lesion in the right breast is increased by 23% in AiCE (2.1 g/ml) compared to OSEM with PSF and GF (1.7 g/ml). A spherical ROI with diameter of 3 cm was drawn in the center of the liver and the coefficient of variation (COV) was measured, which is defined by the ratio of standard deviation and the mean of the ROI. The COV of the liver ROI is decreased by 32% in AiCE (5.2%) compared to OSEM with PSF and GF (7.6%).

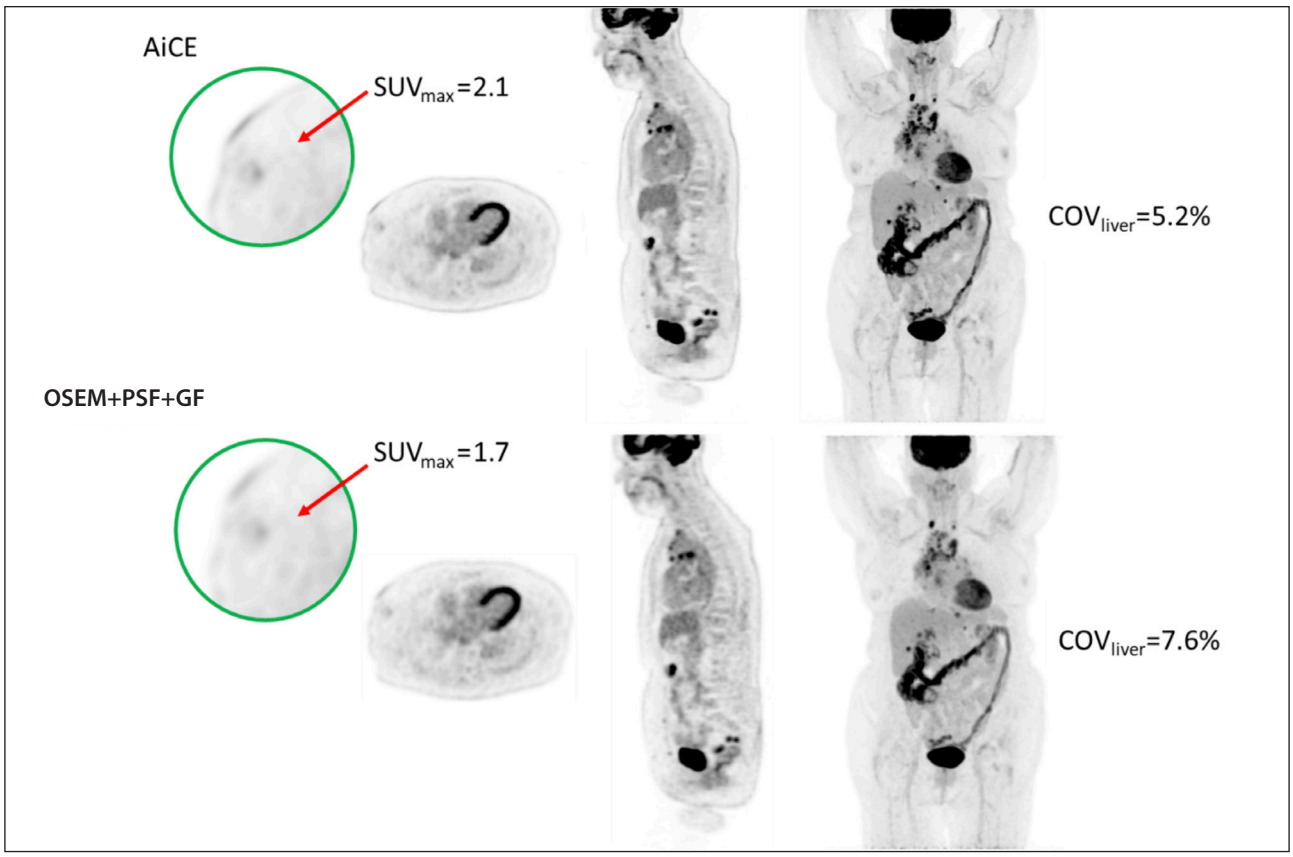

Figure 9 AiCE and OSEM with PSF and GF (OSEM+PSF+GF) images of a patient with large BMI and a low contrast lesion in the outer right breast shown in the zoom-in.

Conclusion

The experience of the Nuclear Medicine imaging field with PET TOF technology, clinically available since the mid-2000s, has demonstrated the benefits of TOF technology. TOF PET can improve SNR, contrast recovery, noise propagation, effective sensitivity, measurement accuracy and precision, and image reconstruction convergence compared to non-TOF PET technology. All these improvements lead to improved image quality and/or reduced scan time.

Using innovative technologies, Cartesion Prime PET/CT has achieved excellent timing resolution and image quality. The presented phantom study demonstrated that for a 35 cm diameter phantom, TOF resulted in faster convergence. CRC at the same noise level was also higher for TOF images acquired by two-minute scans compared non-TOF images acquired by scans that were 5.5 times longer. In addition, incorporating PSF in TOF OSEM reconstructions can improve CRC at the same noise level compared to TOF OSEM reconstructions without PSF. Finally, combining TOF technology with AiCE can further enhance image quality and/or optimize scan times.

Better image quality helps clinicians to better visualize lesions. Optimized scan times can improve workflow and patient comfort. Cartesion Prime provides excellent TOF resolution and its aforementioned benefits combined with 3D listmode TOF OSEM reconstruction with PSF. Canon Medical's AiCE* for PET DLR can also be used to add onto the TOF benefits.

** Option*

References:

1. M. Conti, Focus on time-of-flight PET: the benefits of improved time resolution, Eur J Nucl Med Mol Imaging. 2011 Jun;38(6):1147-57. doi: 10.1007/s00259-010-1711-y. Epub 2011 Jan 13. Erratum in: Eur J Nucl Med Mol Imaging. 2011 Jun;38(6):1171. PMID: 21229244.
2. DJ Kadrmas, ME Casey, M Conti, BW Jakoby, C. Lois, DW Townsend, Impact of time-of-flight on PET tumor detection, J Nucl Med. 2009 Aug;50(8):1315-23. doi: 10.2967/jnumed.109.063016. Epub 2009 Jul 17. PMID: 19617317; PMCID: PMC2786272.
3. S. Surti, JS Karp, Advances in time-of-flight PET, Phys Med. 2016 Jan;32(1):12-22. doi: 10.1016/j.ejmp.2015.12.007. Epub 2016 Jan 6. PMID: 26778577; PMCID: PMC4747834.
4. ME Daube-Witherspoon, S. Surti, AE Perkins, JS Karp, Determination of accuracy and precision of lesion uptake measurements in human subjects with time-of-flight PET, J Nucl Med. 2014 Apr;55(4):602-7. doi: 10.2967/jnumed.113.127035. Epub 2014 Mar 6. PMID: 24604909; PMCID: PMC4128014.
5. C. Lois, B. W. Jakoby, M. J. Long, K. F. Hubner, D. W. Barker, M. E. Casey, M. Conti, V. Y. Panin, D. J. Kadrmas, and D. W. Townsend, An assessment of the impact of incorporating time-of-flight information into clinical PET/CT imaging, J. Nucl. Med., vol. 51, no. 2, pp. 237–245, 2010.
6. X. Li, W. Qi, M. Miyahara, J Kolthammer, Performance Characterization of an SiPM-based Time-of-Flight Canon PET/CT Scanner, *Journal of Nuclear Medicine*, vol. 61, no. supplement 1, pp. 14–14, May 2020.
7. B Bai, M Iatrou, Cartesion Prime: A Well-Balanced Digital PET/CT Scanner [White Paper], Canon Medical Systems USA, Inc., 2020. https://us.medical.canon/products/molecular-imaging/cartesion-prime/#/resources/modals/molecular-imaging/cartesion-prime-wp/
8. T. K. Lewellen, Recent developments in PET detector technology, Phys. Med. Biol., vol. 53, no. 17, p. R287, 2008.
9. W. Moses, *Time of flight in PET revisited, Nucl. Sci. IEEE Trans. On, vol. 50, no. 5, pp. 1325–1330, 2003.*
10. T. Budinger, Time-of-flight positron emission tomography - status relative to conventional PET, J Nucl Med, vol 24, no. 1, pp.73–78, 1983.
11. S. Surti, S. Karp, L. M. Popescu, E. Daube-Witherspoon, and M. Werner, "Investigation of time-of-flight benefit for fully 3-DPET," IEEE Trans Med Imaging, vol. 25, no. 5, pp. 529–538, 2006.
12. G. Mettivier, V. Tabacchini, M. Conti, and P. Russo, Signal-to-noise gain at variable randoms ratio in TOF PET, Nucl. Sci. IEEE Trans. On, vol. 59, no. 5, pp. 1948–1957, 2012.
13. T. Tomitani, Image reconstruction and noise evaluation in photon time-of-flight assisted positron emission tomography, IEEE Trans Nucl Sci., Vol 28, no. 6, pp. 4582–4589, 1981.
14. K. Boedeker, AiCE Deep Learning Reconstruction: Bringing the power of Ultra-High Resolution CT to routine imaging, Canon Medical Systems Corporation, 2019.
15. C. Chan, et al, An Investigation Study of Deep Learning Convolutional Neural Network for Whole-Body PET Denoising, in RSNA, 2018.
16. B. Bai and M. Iatrou, Advanced intelligent Clear-IQ Engine (AiCE) Deep Learning Reconstruction for PET Imaging with Cartesion Prime Digital PET/CT [White Paper], Canon Medical Systems USA, Inc., 2021.

CANON MEDICAL SYSTEMS USA, INC.
https://us.medical.canon

2441 Michelle Drive, Tustin, CA 92780 | 800.421.1968

MIWP14360US

Made For life